Physically Motivated Discretization Methods

A Strategy for Increased Predictiveness

Dana Knoll, Jim Morel, Len Margolin, and Misha Shashkov

Los Alamos is one of the birthplaces of computational science. The need of the weapons program to approximate the solutions of strongly nonlinear, coupled partial differential equations in complex domains has been a continuous driver in the dual development of supercomputing platforms and of more accurate and efficient numerical algorithms. More recently, the cessation of nuclear testing has placed a new requirement on algorithms, that of increased predictiveness.

Despite the importance and magnitude of the effort that has been put into computational science, in many ways the construction of new algorithms remains more of an art than a science. While the accuracy and efficiency of an algorithm can be studied and enhanced with the mathematical tools of numerical analysis, increased predictiveness is more typically the result of incorporating physical principles into the algorithm. In this article, we describe three examples of methodologies for improving predictiveness of numerical simulations: mimetic differencing, asymptotic-preserving discretization, and implicitly balanced solution techniques. The first two methodologies are focused on spatial discretization, and the third, on temporal discretization. Each is attempting to embed some basic underlying physical concept into the numerical method, thereby improving the fidelity and predictive capability of computer simulation. At some level, these methodologies are currently being incorporated in existing or next-generation simulation software within the Los Alamos weapons program.

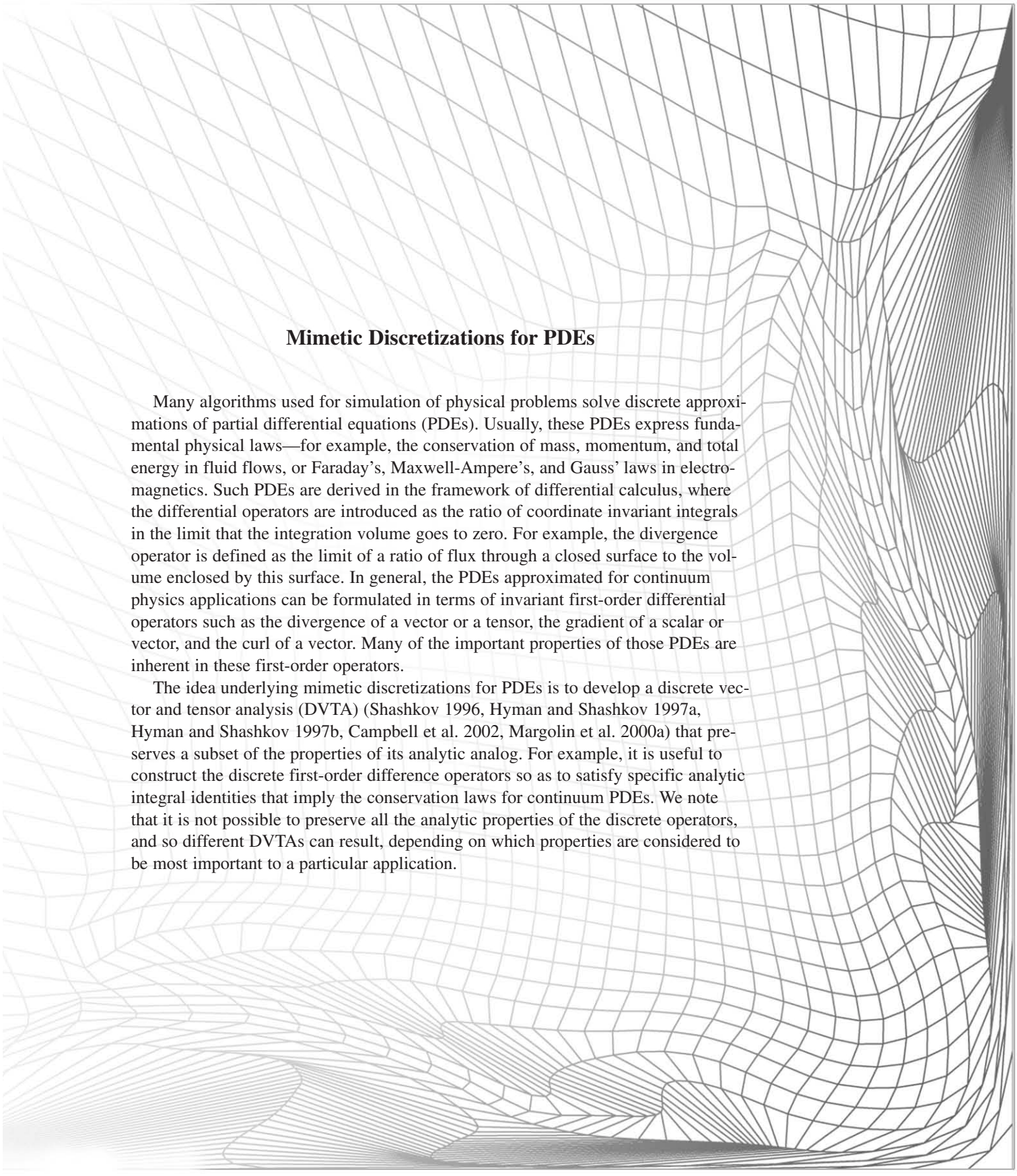

Mimetic Discretizations for PDEs

Many algorithms used for simulation of physical problems solve discrete approximations of partial differential equations (PDEs). Usually, these PDEs express fundamental physical laws—for example, the conservation of mass, momentum, and total energy in fluid flows, or Faraday's, Maxwell-Ampere's, and Gauss' laws in electromagnetics. Such PDEs are derived in the framework of differential calculus, where the differential operators are introduced as the ratio of coordinate invariant integrals in the limit that the integration volume goes to zero. For example, the divergence operator is defined as the limit of a ratio of flux through a closed surface to the volume enclosed by this surface. In general, the PDEs approximated for continuum physics applications can be formulated in terms of invariant first-order differential operators such as the divergence of a vector or a tensor, the gradient of a scalar or vector, and the curl of a vector. Many of the important properties of those PDEs are inherent in these first-order operators.

The idea underlying mimetic discretizations for PDEs is to develop a discrete vector and tensor analysis (DVTA) (Shashkov 1996, Hyman and Shashkov 1997a, Hyman and Shashkov 1997b, Campbell et al. 2002, Margolin et al. 2000a) that preserves a subset of the properties of its analytic analog. For example, it is useful to construct the discrete first-order difference operators so as to satisfy specific analytic integral identities that imply the conservation laws for continuum PDEs. We note that it is not possible to preserve all the analytic properties of the discrete operators, and so different DVTAs can result, depending on which properties are considered to be most important to a particular application.

The construction of a mimetic discretization for a particular PDE starts with the choice of a discrete representation of the scalar and vector fields—what is usually termed the data structure. (Here, we are considering discretizations that employ a computational mesh, which is the most common but by no means the only choice.) For example, in electromagnetics it is natural to choose the normal projections of magnetic flux density with respect to the faces of the computational cells and the normal projections of electric field intensity to edges of the computational cells as primary variables, because these components of the magnetic and electric fields are continuous at an interface between different materials (Hyman and Shashkov 1999a). On the other hand, in Lagrangian gas dynamics, it is natural to locate the Cartesian components of velocity at the nodes of the mesh because, in a Lagrangian framework, the nodes of the mesh move with the fluid (Caramana et al. 1998b).

The next step is to identify the connection between the most significant properties of the model PDEs and the first-order differential operators in terms of which they are written. For example, the conservation of total energy in Lagrangian gas dynamics formally follows from the property that the analytic gradient operator is the negative adjoint of the analytic divergence operator (Shashkov 1996):

$$\int_V p\nabla\cdot\mathbf{W}dV + \int_V \mathbf{W}\cdot\nabla p dV = \oint_{\partial V} p\mathbf{W}\cdot\mathbf{n}dS \quad , \tag{1}$$

where p is the (scalar) pressure and $\mathbf{W}$ is the (vector) velocity field. Similarly,the conservation of momentum in the equations of gas dynamics follows from the following property of the gradient:

$$\int_V \nabla p dV = \oint_{\partial V} p\mathbf{n}dS \quad . \tag{2}$$

A third example arises in solid dynamics, where the velocity derivatives are used to estimate the strain-rate tensor. Here it is important to define the discrete divergence operator so that the divergence of velocity is consistent with the change of volume of a material parcel (Margolin et al. 2000a):

$$\nabla\cdot\mathbf{W} = \lim_{\delta V\to 0}\frac{\frac{d}{dt}(\delta V)}{\delta V} \quad . \tag{3}$$

Sometimes it is not possible to formulate discrete operators that satisfy all of the desired properties; for example, in multidimensional Lagrangian gas dynamics, it is not possible to construct a discretization that simultaneously conserves energy and preserves entropy in smooth isentropic flows.

Conservation is not the only important property to mimic. Another feature of operators, which is closely related to physics, is the associated null space. In the continuum, the gradient of a scalar function can be zero if and only if this function is constant in space; we say that the null space of the gradient operator consists of constants. Similarly, the null space of the analytic divergence operator consists of vectors that can be represented as a curl of another vector field. If the discrete operators have a larger null space than their continuum counterparts, parasitic (that is, unphysical) modes may grow and pollute the numerical solution. For example, in electromagnetics one may see magnetic monopoles (see discussion in Hyman and Shashkov 1999a). In Lagrangian gas dynamics on a two-

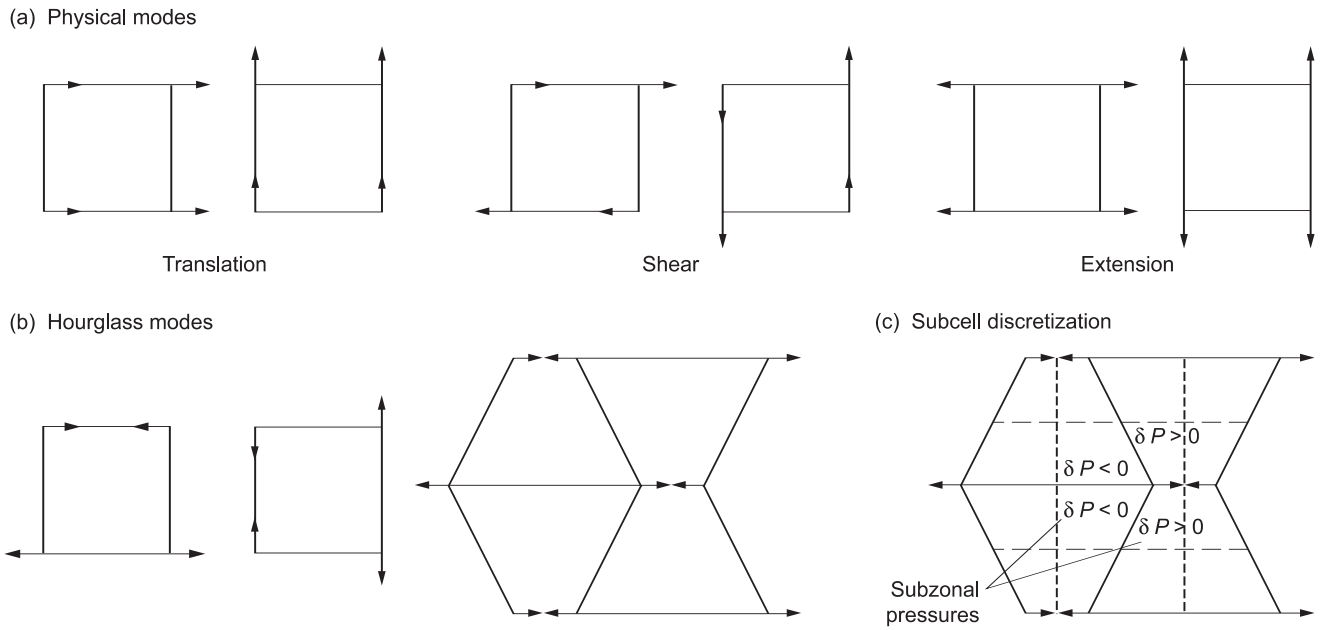

Figure 1. Hourglass Modes
Degrees of freedom that are exhibited by a quadrilateral cell in a Lagrangian mesh are shown in (a) and (b). In addition to physical patterns of motion-translation, extension, shear and rotation, a quadrilateral cell in a Lagrangian mesh can exhibit an unphysical motion called an hourglassing. Because hourglassing neither changes the area of the cell nor does any work on the cell, this pattern produces no restoring forces. Thus, an additional mechanism must be introduced to control the resulting artificial grid distortion. One approach (Margolin and Pyun 1987) to treating hourglassing is to directly filter the pattern from the velocity field. An alternate strategy (Caramana and Shashkov 1998) is to employ a subcell discretization for density (see the dotted lines in Figure 1(c)) that recognizes the consequent hourglass distortion and produces restoring forces (δP in Figure 1(c)).

dimensional (2-D) quadrilateral mesh, one may see so-called hourglassing modes, which distort the shape of the cells without producing restoring forces (refer to Figure 1). This problem is well known in the finite-element community, where it is termed "under-integration;" however, hourglassing patterns are found in finite-difference and finite-volume simulations as well. On the other hand, when the discrete operators have a smaller null space, the solution becomes "stiff," a problem analogous to the well-known phenomenon of locking in finite elements.

The finite size of computational cells leads to another important consideration for mimetic algorithms. While the PDEs can resolve all the scales of motion in a problem, a simulation is more restricted. For example, in high Reynolds number flows, the energy dissipation by molecular viscosity cannot be resolved. The absence of the effects of physical viscosity leads to the need for an artificial mechanism to dissipate a correct amount of energy; in turbulence, this mechanism is called a subgrid-scale model, while in compressible flows with shocks, it is termed an artificial viscosity. Artificial viscosity was first proposed by von Neumann and Richtmyer (1950) to regularize shocks that can not be resolved on the computational mesh. By "regularize," we mean dissipate sufficient energy (and create sufficient entropy) to capture the shock on the mesh without unphysical oscillations. In fluids and gases, the forces due to physical viscosity are isotropic. However, to effectively regularize shocks so that the flow does not depend on the details of the computational mesh, the artificial viscosity needs to have the form of a (possibly nonsymmetric) second-order tensor (Campbell and Shashkov 2001).

In Figure 2, we demonstrate the extent to which a numerical solution can be affected by the choice of mesh if the artificial viscosity is not properly formulated. The simulated problem is known as the Noh implosion and is widely used to study the effects of artificial viscosity. Initial conditions for this problem are specified as a spatially uniform density and an inward radial velocity. The flow has a simple analytic solution, which is an expanding circular shock wave. For the values of density and velocity specified, the position of the shock is at radius

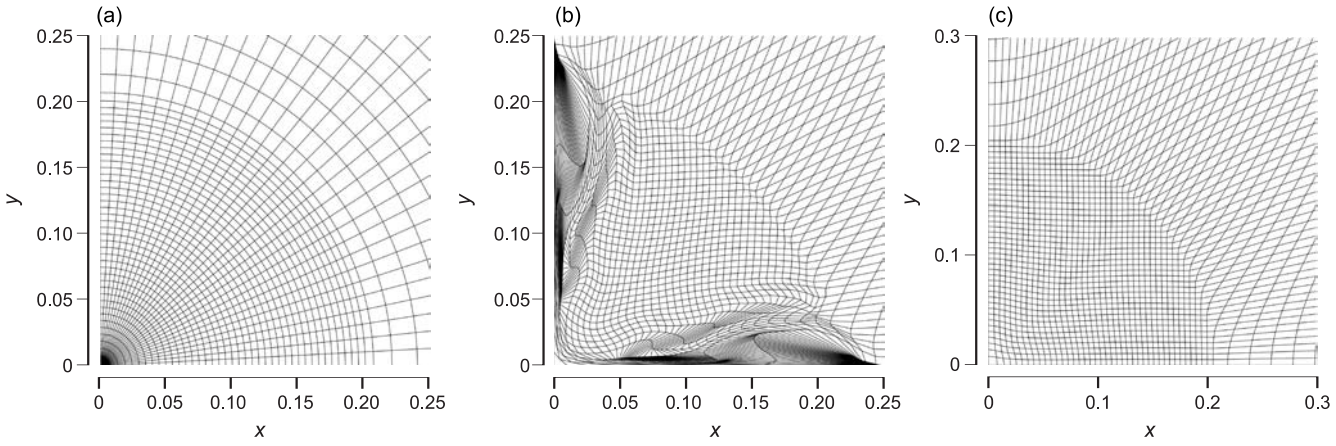

Figure 2. The Effects of the Choice of Mesh and of Artificial Viscosity on an Implosion Problem

(a) Results using an initial mesh with polar symmetry that anticipates the converging fluid flow of a radial implosion. The simulation employs an edge artificial viscosity. The figure shows the simulation is in excellent agreement with the analytic solution at time $t = 0.6$. (b) Results using the same edge viscosity as in panel (a) but starting from a square mesh produces asymmetric results by $t = 0.6$. (c) Results using a tensor artificial velocity and starting with an initially square mesh produces superior results at $t = 0.6$.

$R = 0.2$ for time $t = 0.6$. Now, in Lagrangian simulations, best results are typically obtained when the symmetry of the flow coincides with the symmetry of the mesh. Unfortunately, in realistic problems such a choice of mesh is not always possible. To illustrate these points, we present results for two types of initial mesh: A polar mesh that reflects the anticipated symmetry of the flow is shown in Figure 2(a), and a uniform square mesh is shown in Figures 2(b) and 2(c). Two types of artificial viscosity are used, an "edge viscosity" (Caramana et al. 1998a), as illustrated in Figures 2(a) and 2(b), and a tensor viscosity (Campbell and Shashkov 2001), shown in Figure 2(c). The edge artificial viscosity works well for the initial polar mesh, which is aligned with flow—see Figure 2(a)—but performs poorly for the initial square mesh shown in Figure 2(b), which is not aligned with flow. The reason for such behavior is that the forces generated by the artificial edge viscosity depend strongly on mesh. The tensor artificial viscosity is based on a mimetic discretization of the gradient of a velocity. Because this gradient is based on the discretization of a coordinate invariant differential operator, it is able to produce results that show essentially no dependence on the mesh—see Figure 2(c).

The preservation of the physical flow symmetry in an implosion is critically important to achieve accurate predictions for the inertial confinement fusion program. Small departures from spherical symmetry due to discrete errors can grow into unacceptably large asymmetries in systems undergoing strong convergence. Also, the uncertainty of whether a nonsymmetric result is due to numerical errors or to the physical design severely limits our predictive capability and ultimately our understanding of the dynamical behavior of an implosion. Those methods that preserve symmetries are viable for investigating perturbations of these symmetries. However, the development of such methods may require consideration of meshes with curvilinear edges (as opposed to straight line segments) and the derivation of discrete operators on such a mesh (Margolin and Shashkov 1999, Margolin et al. 2000b). An alternative approach on a line segment mesh has been developed based on the addition of special corrective forces (Caramana and Whalen 1998).

We demonstrate the importance of using symmetry-preserving discretizations on a spherical version of the Rayleigh-Taylor instability (Margolin et al. 2000b). Radial gravity is assumed to act on an unstable interface placed at radius $R = 1$. The computational domain is $.25 \le R \le 1.75$. We use a γ-law gas as the equation of state, with $\gamma = 1.4$. The initial velocity for all nodes is zero. The density is 100.0 for $R > 1$ and 1.0 for $R < 1$. The initial pressures are chosen to be in exact hydrostatic balance. The gravitational constant is taken as 0.02.

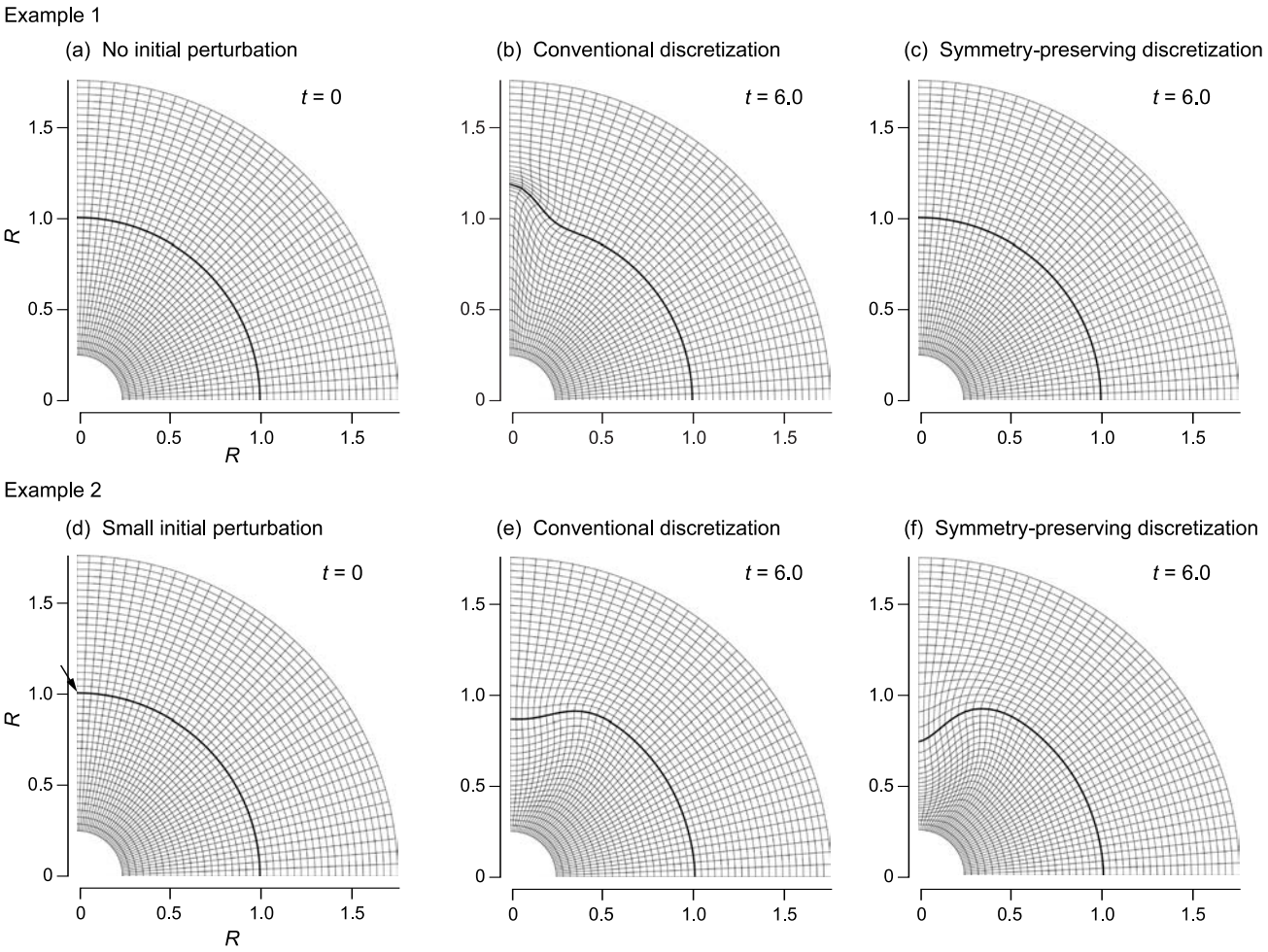

Figure 3. The Effects of Symmetry-Preserving Discretization in the Simulation of a Spherical Rayleigh-Taylor Instability

(a) An interface at $R = 1$ initially separates a dense outer fluid from a less-dense inner fluid. Both fluids are in a gravitational field directed radially inward. (b) With no initial perturbation at the fluid interface, the solution obtained by differencing on a line-segment mesh (Caramana et al. 1998c) develops an unphysical instability by $t = 6.0$. (c) With the same initial conditions, the solution at $t = 6.0$ obtained by differencing on a curvilinear mesh (Margolin and Shashkov 1999) is unchanged from that at $t = 0$ (as expected). (d) The initial mesh is slightly perturbed at the north pole. (e) The solution obtained by differencing on a line-segment mesh shows an instability whose maximum growth rate is not along the vertical axis at $t = 6.0$, which is incorrect. (f) The solution obtained using a curvilinear mesh and with the same initial perturbation as in panel (d) produces an instability whose maximum growth rate is along the vertical axis at $t = 6.0$, which is qualitatively correct.

In the first example shown in Figure 3, the initial state—refer to Figure 3(a)—is represented on a polar grid without any initial perturbation. When a conventional discretization scheme is used (Caramana et al. 1998b), an asymmetric truncation error quickly triggers an instability and, by time $t = 6$, has produced the unphysical mode shown in Figure 3(b). The symmetry-preserving scheme does not trigger any instability. Therefore, the solution at $t = 6$ shown in Figure 3(c) is unchanged from the initial condition in Figure 3(a).

The second example employs a grid with a very small initial perturbation (not visible to the naked eye) at $R = 1$—see Figure 3(d). Let θ_i be the usual angle in

the $r - z$ plane of the points along $R = 1$ in the unperturbed grid. The perturbed grid replaces these points with $r_i = (1 + \mathrm{f}(\theta_i))\cos(\theta_i)$ and $z_i = (1 + f(\theta_i))\sin(\theta_i)$. The perturbation f is designed to produce a very small indentation centered at the north pole. The exact form is given by

$$f = -.002\left(1 + 6.5\left(\frac{\pi}{2} - \theta_i\right)^2\right)^{-1} \quad . \tag{4}$$

The solution that uses a conventional scheme is shown in Figure 3(e). It is visibly different from that produced by the symmetry-preserving scheme. The maximum growth rate for the conventional scheme is no longer along the z-axis, even though the initial perturbation is largest at the z-axis.

The solution at time $t = 6$ for this case, using mimetic differencing on curvilinear mesh, is shown in Figure 3(f). It exhibits the expected growth of the initial perturbation. The maximum growth rate is along the z-axis, where the initial perturbation is largest.

As previously noted, the construction of discrete operators and the overall properties of discrete algorithms depend significantly on the choice of the computational mesh. In addition to trying to coordinate the mesh symmetry with the expected symmetry of the flow, it is found that aligning the mesh with material interfaces (Hyman et al. 2002) and having orthogonality of the mesh lines to the interface (Khamayseh and Hansen 2000) are also key to improving the accuracy of simulations. Further, the overall accuracy of an algorithm also depends on the smoothness of the mesh. (A mesh is smooth if such characteristics as the volumes of the cells and the lengths of the cell edges vary smoothly in the mesh—refer to Knupp et al. 2002.)

In Lagrangian simulations, there is no guarantee that an initially smooth mesh will remain smooth. For this reason, a hybrid technique named arbitrary Lagrangian-Eulerian, or ALE, has been developed (Margolin 1997) to allow the automatic identification and improvement of Lagrangian meshes during the simulation. ALE techniques require a strategy for how to rezone (that is, improve) a nonsmooth or tangled mesh. Some elements of this strategy are to preserve the integrity of interfaces and other physically important surfaces (Garimella et al. 2004) and to try to "mass match," that is, to make the mass of the cells vary smoothly in space. However, formulating more general and more complete strategies for rezoning, which simultaneously improve mesh quality while enhancing solution accuracy, is an active field of research.

There are many other issues to consider in the design of discrete operators. For example, for the implicit discretization of a diffusion equation, one needs to solve a system of linear (or perhaps nonlinear) equations. The continuum diffusion operator is symmetric and positive-definite (SPD). If the discrete gradient and divergence are negatively adjoint to each other, then the discrete diffusion operator is also SPD (Hyman et al. 2002). Such SPD operators have the practical advantage that there exist efficient iterative solvers for the associated matrix equations.

To summarize, we have illustrated that many of the important properties of the PDEs that describe the evolution of physical processes are inherent in the differential operators from which they are constructed. We have given examples of how to design discrete operators that mimic these important properties of their analytic counterparts. In some cases, these properties transcend the individual discrete operators and require relationships between different operators to be enforced. We offer that our approach of a discrete tensor and vector analysis pro-

vides a formal framework to study the convergence, symmetries, and accuracy of numerical methods (Berndt et al. 2001). At the same time, we recognize that this is an unfinished story and much work remains to be done.

Balanced Approximations for Time Integration of Multiple-Time-Scale Systems

It can be quite a challenge to do numerical modeling of physical systems that involve many processes occurring at different speeds. The faster processes must be resolved by small simulation time steps, which is computationally expensive, or must be modeled by other means.

Often, the faster processes are nearly in balance at all times, and the system as a whole evolves more slowly than any of the faster processes. A classic example of this type of situation is the flame speed of a laminar diffusion flame. The diffusion and reaction at the flame front are fast processes. However, they compete with each other, with one process slightly dominating the other. The two processes are nearly in balance, producing a flame front that propagates relatively slowly. This is the type of multiple-time-scale problem considered here. There are many examples of such problems in plasma physics, geophysical fluid dynamics, combustion, and radiation hydrodynamics (see, for example, Brackbill and Cohen 1985).

For these problems, it is computationally efficient to resolve only the relatively slow evolution of the system as a whole by using a time step that is large compared with the time scales of the faster processes. At the same time, one must preserve the dynamical balance responsible for the slow evolution of the system. An effective way to achieve this result is to design nonlinear, implicit time-integration schemes that ensure a consistent solution of the separate processes even when large time steps are used. We call such techniques implicitly balanced (Knoll et al. 2003). These techniques were avoided in the past because of a lack of efficient implicit solvers. At that time, formulations based on time splitting and/or linearization were mainly used (Brackbill and Cohen 1985).

In this article, we demonstrate that (1) split methods contain inherent errors that could be dangerous for predictive simulation, (2) modified equation analysis (MEA) (Hirt 1968, Warming and Hyett 1974) can identify possible errors in split methods, and (3) modern, implicitly balanced methods can provide efficient alternatives to split methods. The second point is important because some form of time splitting is required for many problems of interest. We demonstrate these three points by using simple numerical experiments and numerical analysis.

First, we show how MEA can identify splitting errors. The classical analysis of splitting and linearization errors uses asymptotic expansions of exponential operators (Strang 1968). The technique is well suited to determining the stability and assessing the order of accuracy (that is, the rate of convergence) of time-split algorithms. However, the analysis is less useful for obtaining quantitative estimates of the consequences of linearization, the effects of boundary conditions, or the error itself. The latter items can be more readily obtained using MEA, in which a Taylor-series truncation analysis is applied to the discretized PDE (or semidiscretized PDE, for the example considered here). The continuum PDE is reassembled on the left side of the equation, and all the other terms are brought to the right side. This is the new, or modified, equation used for MEA.

Let us now define an implicitly balanced method and compare it with a time-split method, using the equation for the time-dependent reaction-diffusion problem

$$\frac{d\mathbf{u}}{dt} = \mathcal{D}_{\mathbf{u}}\mathbf{u} + \mathcal{R}_{\mathbf{u}}\mathbf{u} \quad , \tag{5}$$

where $\mathbf{u}$ is the dependent variable (or perhaps a system of dependent variables), t is time, $\mathcal{D}_{\mathbf{u}}$ represents the spatial discretization of a diffusion term, and $\mathcal{R}_{\mathbf{u}}$ represents the volumetric reaction, with both $\mathcal{D}_{\mathbf{u}}$ and $\mathcal{R}_{\mathbf{u}}$ being functions of $\mathbf{u}$. In an implicitly balanced method, $\mathcal{R}_{\mathbf{u}}\mathbf{u}$ and $\mathcal{D}_{\mathbf{u}}\mathbf{u}$ will be evaluated at the same value of $\mathbf{u}$ when advancing $\mathbf{u}$ in time. This evaluation is not done with a linearized time-split method.

We wish to advance the solution one discrete time step from the existing time level $\mathbf{u}^n$ to the new time level $\mathbf{u}^{n+1}$. A standard first-order linearized time-split method advances the solution using two linearized subsystems:

$$\frac{\mathbf{u}^* - \mathbf{u}^n}{\Delta t} = \mathcal{D}_{\mathbf{u}}^n \mathbf{u}^* \tag{6}$$

and

$$\frac{\tilde{\mathbf{u}}^{n+1} - \mathbf{u}^*}{\Delta t} = \mathcal{R}_{\mathbf{u}}^n \tilde{\mathbf{u}}^{n+1} \quad , \tag{7}$$

where $\mathbf{u}^*$ is an intermediate, or temporary, value for $\mathbf{u}$. The effective time step is then given by

$$\frac{\tilde{\mathbf{u}}^{n+1} - \mathbf{u}^n}{\Delta t} = \mathcal{D}_{\mathbf{u}}^n \mathbf{u}^* + \mathcal{R}_{\mathbf{u}}^n \tilde{\mathbf{u}}^{n+1} \quad , \tag{8}$$

The linearization that has occurred here is in evaluating $\mathcal{D}_{\mathbf{u}}$ and $\mathcal{R}_{\mathbf{u}}$ at the known values of $\mathbf{u}$, $\mathbf{u}^n$.

One possible second-order-accurate implicitly balanced approach would be

$$\frac{\mathbf{u}^{n+1} - \mathbf{u}^n}{\Delta t} = \mathcal{D}_{\mathbf{u}}^{n+\frac{1}{2}} \mathbf{u}^{n+\frac{1}{2}} + \mathcal{R}_{\mathbf{u}}^{n+\frac{1}{2}} \mathbf{u}^{n+\frac{1}{2}} \quad . \tag{9}$$

The solution of this time discretization will require a nonlinear iteration involving both diffusion and reaction. It is clear that given the same initial value, $\mathbf{u}^n$, these two methods do not give the same final value at the new time level, that is, $\tilde{\mathbf{u}}^{n+1} \neq \mathbf{u}^{n+1}$. We need to understand when this difference is important for predictive simulation.

We will compare and contrast implicitly balanced methods with a simple linearized time-split method using numerical analysis and numerical experiments with a simple model problem. For further details on this discussion, refer to Knoll et al. (2003). In the following paragraphs, we touch only on issues related to splitting, not on those related to linearization.

We consider only the simplest first-order splitting to illustrate the important points. It is straightforward to design a second-order-accurate splitting for the problem considered below. MEA analysis of more sophisticated splittings is ongoing.

We consider the linear reaction-diffusion problem with T as the scalar dependent variable, a constant diffusivity D, and a constant reactivity $\alpha < 0$:

$$\frac{\partial T}{\partial t} - D\frac{\partial^2 T}{\partial x^2} = \alpha T \ , \tag{10}$$

with standard boundary conditions and initial conditions. The dynamical time scale is estimated to be

$$\frac{1}{\tau_{\text{dyn}}} \equiv \left|\frac{1}{T}\frac{dT}{dt}\right| \approx \frac{1}{\tau_{\text{dif}}} + \frac{1}{\tau_{\text{reac}}} \ , \tag{11}$$

where the diffusion time τ_{dif} and reaction time τ_{reac} are

$$\tau_{\text{dif}} \equiv \frac{L^2}{D}; \tau_{\text{reac}} \equiv \left|\frac{1}{\alpha}\right| \ ,$$

and L is the gradient scale of the solution.

To solve Equation (10), we consider a first-order time-split method that first advances the reaction and then the diffusion. Specifically, the first-order splitting is

$$\frac{T^* - T^n}{\Delta t} = \alpha T^* \ , \text{ and}$$

$$\frac{T^{n+1} - T^*}{\Delta t} - D\left(\frac{\partial^2 T^{n+1}}{\partial x^2}\right) = 0 \ , \tag{12}$$

where T^* is an intermediate value for T.

We also consider two balanced methods: one first- and the other second-order accurate. The first-order accurate balanced method is

$$\frac{T^{n+1} - T^n}{\Delta t} - D\left(\frac{\partial^2 T^{n+1}}{\partial x^2}\right) = \alpha T^{n+1} \ . \tag{13}$$

The second-order accurate balanced method is

$$\frac{T^{n+1} - T^n}{\Delta t} - D\left(\frac{\partial^2 T^{n+\frac{1}{2}}}{\partial x^2}\right) = \alpha T^{n+\frac{1}{2}} \ , \tag{14}$$

where the intermediate time is defined as,

$$T^{n+\frac{1}{2}} \equiv \frac{T^{n+1} + T^{n}}{2} \quad . \tag{15}$$

Considering the semidiscrete problem in time (that is, ignoring the spatial discretization), we require the Taylor series expansion of T^n in terms of T^{n+1}:

$$T^{n} = T^{n+1} - \Delta t T_t + \frac{\Delta t^2}{2} T_{tt} - \ldots \quad , \tag{16}$$

where $T_t = \partial T/\partial t$. It is straightforward to show that the modified equation for the first-order accurate balanced method is

$$\left[T_t - D\left(\frac{\partial^2 T}{\partial x^2} \right) - \alpha T \right] = \frac{\Delta t}{2} T_{tt} + O\left(\Delta t^2 \right) \tag{17}$$

and for the second-order accurate balanced method is

$$\left[T_t - D\left(\frac{\partial^2 T}{\partial x^2} \right) - \alpha T \right] = \frac{\Delta t^2}{24} T_{ttt} + O\left(\Delta t^3 \right) \quad . \tag{18}$$

MEA tells us that, when Equation (10) is numerically integrated in time using Equation (13), one is really solving Equation (17). Defining the modified equation for the split method is more subtle.

After the two steps from the split method in Equation (12) have been combined, the effective time step is given by

$$\frac{T^{n+1} - T^{n}}{\Delta t} - D\left(\frac{\partial^2 T^{n+1}}{\partial x^2} \right) = \alpha T^{*} \quad . \tag{19}$$

To perform the MEA, we must eliminate T^n and T^* in favor of T^{n+1} and its time derivatives. As we have seen, T^n can be eliminated using standard Taylor-series expansion. Rather than attempting to write a similar Taylor series for T^*, we can use the second step in the split method itself:

$$T^{*} = T^{n+1} - \Delta t D\left(\frac{\partial^2 T^{n+1}}{\partial x^2} \right) \quad . \tag{20}$$

The modified equation for the splitting method can now be written as

$$\left[T_t - D\left(\frac{\partial^2 T}{\partial x^2} \right) - \alpha T \right] = \frac{\Delta t}{2} T_{tt} \underbrace{- \Delta t \alpha D\left(\frac{\partial^2 T}{\partial x^2} \right)}_{\text{New truncation term}} + O\left(\Delta t^2 \right) \quad . \tag{21}$$

Compared with the first-order balanced method, namely, Equation (17), a new first-order truncation term has appeared in the split modified equation. This new

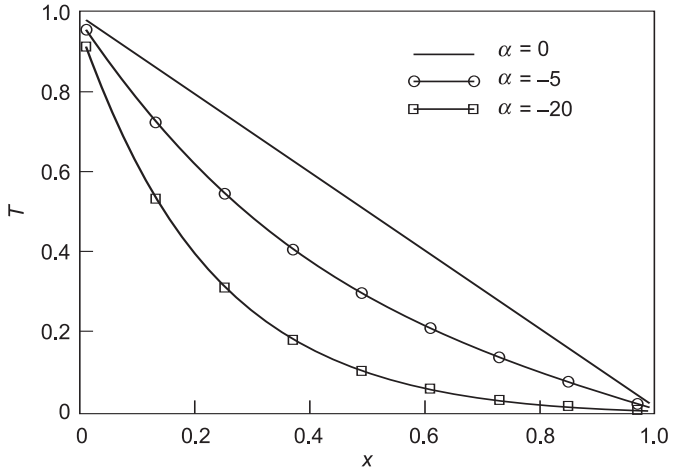

Figure 4. Steady-State Solutions Obtained with the Implicitly Balanced Method

These solutions of the linear reaction-diffusion equation—refer to Equation (10)—were obtained with a second-order-accurate implicitly balanced method. *T* is the scalar dependent variable, and *x* is position. Shown are the solutions for three values of constant reactivity α.

term is proportional to the second spatial derivative and scales with $\alpha\,\Delta t$. If an altered diffusion coefficient is used, the modified equation of the split method can be viewed as having the same form as the modified equation of the balanced first-order-accurate method. Indeed, if we replace D with D^* in Equation (21) and equate terms with Equation (17), the result is

$$D^* = \frac{D}{1.0 - \Delta t\alpha} \quad . \tag{22}$$

This suggests that using the split algorithm with the diffusion coefficient D* should reproduce the results of using the first-order-accurate balanced method with the original diffusion coefficient D. For $\alpha < 0$, the altered diffusion coefficient remains positive and less than the original coefficient.

We consider the problem on the domain $0 < x < 1$ with initial conditions $T(x, t = 0) = 0.1$, $T(x = 0, t) = 1$, $T(x = 1, t) = 0.1$, $D = 1$, $\alpha = -20$, and a time step, Δt, of 0.01. To demonstrate some properties of the solution, we have simulated the problem using the second-order-accurate balanced method with $\Delta t = 0.0001$ and $\alpha = -0$, –5, and –20. Figure 4 shows how different values of the finite reaction term α affect the steady-state solutions. Figure 5 shows the time-dependent solutions at $x = 0.1$. At early times, the dynamical time scale is dominated by the diffusion time scale, τ_{dif}, since L is very small near $x = 0$ (the initial gradient is sharp). As this initial structure fades, the impact of finite α on the evolution of the solution becomes clear.

A study of the time-step convergence, verifying that the simple split method is indeed first-order accurate, is given in Knoll et al. (2003). However, it is not apparent from this study that the split method will give the correct steady-state solution using a large time step—that is, $\alpha\Delta t \approx \mathcal{O}(1)$. Figure 6 shows the solutions as functions of time at a particular point ($x = 0.1$) for the different solution methods. For a time step chosen so that $\alpha\Delta t = 0.2$, the split method does not give the correct steady-state solution. The solution from the split method gives no indication of error since the method is stable and qualitatively correct.

In Figure 7, we show the time history of the solution at the same point ($x = 0.1$) for the first-order balanced method and for the split method with the modified diffusion coefficient D^* given in Equation (22). These two solutions are identical, confirming the validity of the MEA of the splitting errors. From these results, it is evident that the solutions given by these first-order split methods can be interpreted as solutions from a balanced method using an altered diffusion

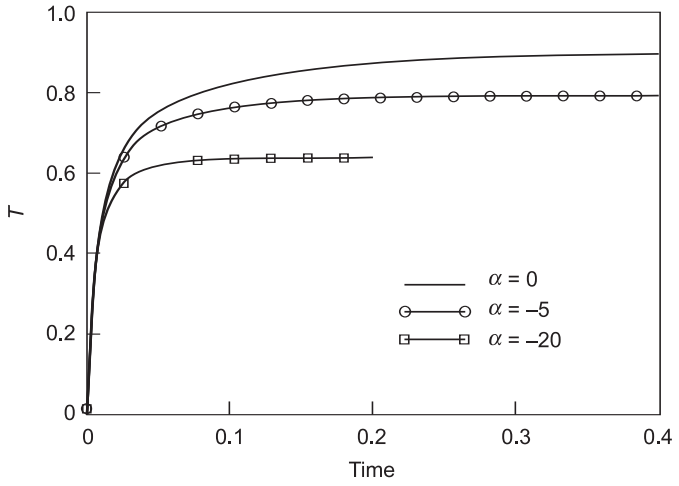

Figure 5. Time-Dependent Solutions Obtained with the Implicitly Balanced Method
These time-dependent solutions to Equation (10) at $x = 0.1$ correspond to the steady-state solutions shown in Figure 4.

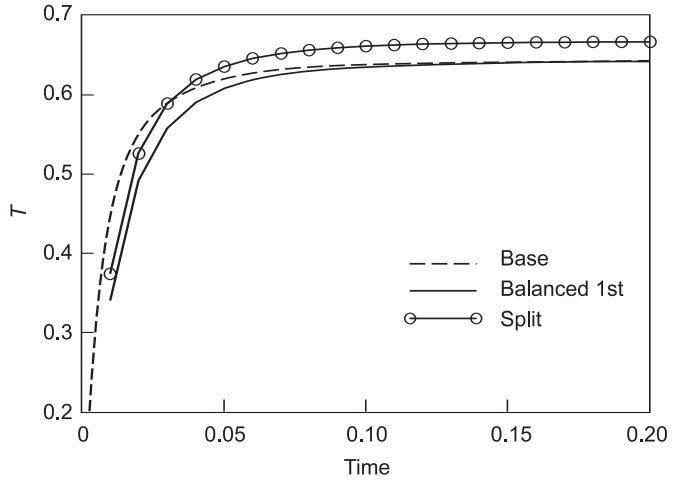

Figure 6. Implicitly Balanced Solutions vs a Split Solution
We compare the time-dependent solutions to Equation (10) at $x = 0.1$ using a second-order-accurate implicitly balanced method ("Base"), a first-order-accurate implicitly balanced method ("Balanced 1st"), and a split method ("Split").

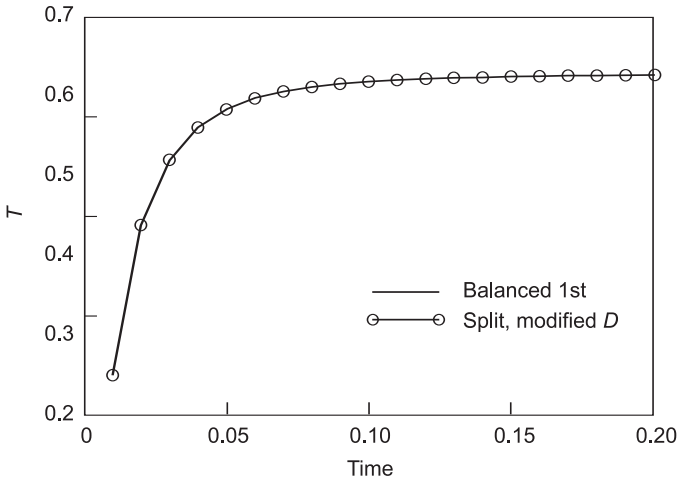

Figure 7. Equivalence of the First-Order-Accurate Balanced Solution and the Split Solution
The solution to Equation (10) obtained with the first-order-accurate balanced method and the original diffusion coefficient ("Balanced, 1st") is identical to the solution obtained with the split method and the corrected diffusion coefficient ("Split, modified D"). The original and corrected diffusion coefficients are related through Equation (22).

coefficient. The degree to which the diffusion coefficient is altered is proportional to the chosen time step normalized by a normal mode (fast) time scale, that is, $\alpha\Delta t = \Delta t/\tau_{\text{reac}}$.

Developing implicitly balanced methods that can be used to simulate large

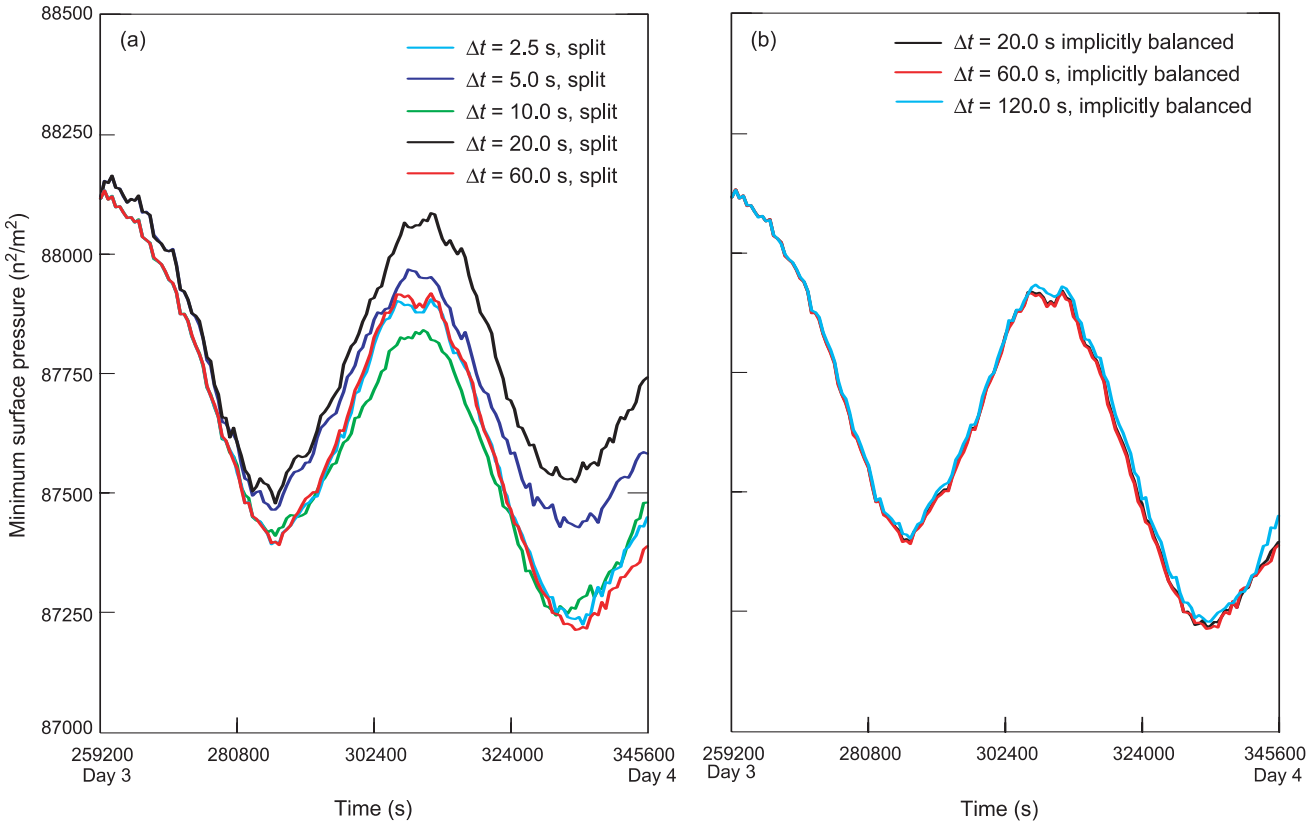

Figure 8. Solution Convergences for the Balanced and Split Methods

We used a 3-D simulation of the minimum pressure in the eye of a hurricane to compare the convergences of (a) split-linearized solutions for different values of the time step (Δt) and (b) implicitly balanced solutions.

three-dimensional (3-D) multiphysics problems is an ongoing research effort that involves many contributors. To give one example, work in this area is discussed in Knoll and Keyes (2004).

Another way to remove the splitting errors is by iterating on the splitting methods. Although some 3-D multiphysics problems have been simulated with implicitly balanced methods, time splitting and linearization are still required for many problems. Thus, we must gain a deeper understanding of the inherent error in time splitting and linearization to achieve more accurate simulations.

Finally, we present results from research using implicitly balanced methods to simulate hurricane intensification (Mousseau et al. 2002, Reisner et al. 2003, Reisner et al. 2004). This 3-D work involves the simulation of compressible multiphase flow. Hurricanes intensify by passing over warm water, and the signature of intensification is the minimum pressure in the hurricane eye. In Reisner et al. (2004), an initially steady-state hurricane is driven into a transient state by specific time-dependent boundary conditions, namely, a time-varying temperature at the ocean's surface. The dynamical time scale in this problem is estimated to be roughly 100 seconds, whereas the sound-wave time scale is roughly 1 second. The split-linearized method, therefore, is used on sound-wave physics equations. Figure 8 shows that, for the implicitly balanced method, the correct solution converges for a time step of $\Delta t = 60$ seconds, whereas the split-linearized method requires a time step of $\Delta t = 1$ second to achieve convergence. In this article, the implicitly balanced method achieved convergence about 5 times faster than the split-linearized method.

Asymptotic-Preserving Discretization Schemes

Asymptotic limits associated with PDEs are limits in which certain terms in an equation are purposely made "small" relative to other terms. Such limits reflect physical situations in which certain physical quantities or processes do, in fact, dominate others. For instance, the compressible hydrodynamic Euler equations, which describe inviscid fluid flow, represent an asymptotic limit of the nonlinear Boltzmann equation for rarefied gas dynamics. In that limit, the ratio of the mean distance between atomic collisions to the system size goes to zero. Similarly, the equations for incompressible fluid flow can be derived from the compressible Euler equations in the limit as the ratio of the material speed to the speed of sound in the material goes to zero. Although asymptotic equations approximate the equations from which they are derived, they accurately represent system behaviors for problems that are highly asymptotic.

An asymptotic equation emerges from the process for obtaining a formal asymptotic solution. The mathematical procedure for obtaining such a solution introduces an asymptotic dimensionless scaling parameter ε that tends to zero. First, the original, or parent, equation is put in dimensionless form, and some of the terms in the equation are scaled by ε^n, where n is a positive integer that may take on different values for different terms. This scaling is defined so that the equation has the desired asymptotic physical behavior as ε goes to zero. Once the scaling is completed, the equation is returned to dimensional form, and the asymptotic solution is assumed to take the form of a power series expansion in ε. This expansion is substituted into the scaled equation, and coefficients of like powers of ε are equated, thereby forming a hierarchical set of equations for the expansion coefficients. The expansion coefficient associated with the lowest power of ε represents the asymptotic solution, that is, the solution obtained in the limit as ε goes to zero. One can use the hierarchical equations to deduce the equation satisfied by the asymptotic solution and thereby obtain the asymptotic equation.

Because the asymptotic equation is generally simpler than the parent equation, it is easier to solve the asymptotic equation for the problems for which it applies than to solve the parent equation. The applicable problems are those in which the assumed dominance of certain terms occurs to a significant extent. Of course, no real problem is perfectly asymptotic, but the exact limit can be approached as closely as desired. As a problem becomes increasingly asymptotic, the solution of the asymptotic equation approaches the solution of the parent equation. However, many problems that require numerical solutions have spatial regions that change in time from asymptotic to nonasymptotic. In those cases, it is often impractical to solve the parent equation in nonasymptotic regions and the asymptotic equation in asymptotic regions. Thus, one must obtain solutions in both the nonasymptotic and asymptotic regions using a single numerical approximation to the parent equation. For the approximation scheme to be valid, solutions to the discrete equation must converge to the continuum solutions as the mesh size goes to zero in both asymptotic and nonasymptotic regions. The problem is that not all methods of discretizing the parent equation produce solutions that converge appropriately in the asymptotic regions. On the contrary, for some discretization schemes, an accurate asymptotic solution is obtained only if the mesh size h resolves length scales much smaller than those relevant to the asymptotic solution. We call such schemes nonasymptotic preserving. Such schemes are inefficient in highly asymptotic regions because they require an excessively large number of spatial cells. In fact, nonasymptotic-preserving schemes require an infinite number of cells in the limit as a region becomes perfectly asymptotic.

To determine whether a discretization scheme "preserves" the asymptotic limit (that is, converges appropriately to the asymptotic solution), one must perform and analyze an asymptotic expansion for the discrete equation that is completely analogous to the expansion for the continuum equation. In this article, we use a particle transport equation and the asymptotic diffusion limit associated with this equation to illustrate both the continuum and discrete asymptotic methodologies. The asymptotic diffusion limit of particle transport is characterized by negligible particle absorption and a diffusion length that is large relative to the mean free path (or average distance between collisions). We derive the diffusion limit for the continuum transport equation and then apply the asymptotic methodology to two spatially discrete forms of the transport equation. One form is obtained using the diamond discretization scheme, and the other is obtained using the upwind discretization scheme. We show that the diamond scheme is asymptotic preserving and the upwind scheme is not. Finally, we give specific computational examples demonstrating the contrasting behavior of these schemes in highly asymptotic (diffusive) problems.

We focus our discussion on a particle transport equation:

$$\mu \frac{\partial vN}{\partial x} + (\sigma_a + \sigma_s)\, vN = \frac{\sigma_s}{2} \int_{-1}^{+1} vN(x,\mu')\, d\mu' + Q \quad . \tag{23}$$

This is an equation for a phase-space particle-density function, $N(x, \mu)$. Although this function depends on a single spatial coordinate, its domain is 3-D and corresponds to an infinite slab. All particles travel at a single speed, v, in directions characterized by the cosine $\mu = v_x/v$. Each cosine corresponds to a cone of directions as illustrated in Figure 9. Particles are assumed to be uniformly distributed within the band. The number of particles located at position x in direction μ, is $N(x, \mu)\, dx\, d\mu$. The spatial volume associated with dx has unit dimensions in the other two Cartesian coordinates, that is, it consists of a differential rectangular box with dimensions $dx \times 1 \times 1$. Particles are randomly absorbed and scattered within the medium. The scattering is isotropic, that is, particles scatter into all directions with equal probability. The absorption cross section is σ_a, and the scattering cross section is σ_s. The expected absorption rate of particles in direction μ at position x is $\sigma_a vN(x, \mu)\, dx\, d\mu$, and the expected scattering rate of particles in direction μ at position x is $\sigma_s vN(x, \mu)\, dx\, d\mu$. The total cross section, σ_t, is the sum of the absorption and scattering cross sections. The mean distance between particle interactions is called the mean free path, and it is given by $\lambda_t = 1/\sigma_t$. The mean free path represents a fundamental spatial scale length in highly absorbing media that appears explicitly in the transport equation. For instance, after traveling a distance s in a purely absorbing medium, a beam of particles is attenuated by a factor of $\exp(-s/\lambda_t)$. The quantity $Q(x,\mu)$ is the particle source function. Therefore, the number of particles created at position x in direction μ is $Q(x,\mu)\, dx\, d\mu$.

Equation (23) is a statement of particle conservation. It simply states that the source rate for the particles entering the differential phase-space volume at position x and direction μ must equal the sink rate for the particles leaving that volume. The boundary conditions for Equation (23) are given in terms of the incident particle distributions at the boundaries. For instance, if the problem domain is the interval [0, 1], the solution to Equation (23) is uniquely determined once N is defined at $x = 0$ for $\mu > 0$ and at $x = 1$ for $\mu < 0$.

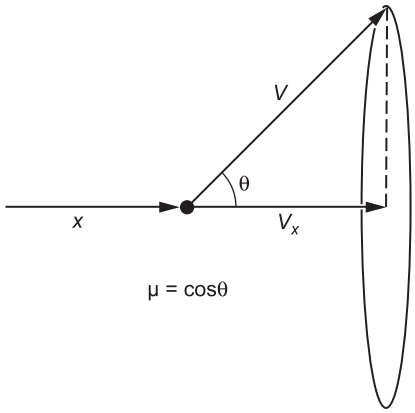

Figure 9. Variable Definitions for the Particle-Density Function $N(x, \mu)$
The number of particles at position x moving in direction μ is $N(x, \mu)\, dx\, d\mu$.

It is convenient for our purposes to rewrite Equation (23) as

$$\mu \frac{\partial \psi}{\partial x} + \sigma_t \psi = (\sigma_t - \sigma_a)\phi + Q \quad , \tag{24}$$

where

$$\phi = \frac{1}{2} \int_{-1}^{+1} \psi(x,\mu')d\mu' \quad . \tag{25}$$

The quantity $\psi = vN$ is called the angular flux, and the directional average of ψ, which is denoted by ϕ, is called the scalar flux.

We now begin the derivation of the asymptotic diffusion limit associated with Equation (24). For simplicity, we skip the nondimensionalization process and directly scale Equation (24) by the nondimensional scaling parameter ε:

$$\mu \frac{\partial \psi}{\partial x} + \frac{\sigma_t}{\varepsilon} \psi = \left(\frac{\sigma_t}{\varepsilon} - \varepsilon \sigma_a \right) \phi + \varepsilon Q \quad . \tag{26}$$

Scaling the terms in Equation (24) ensures the following behavior as $\varepsilon \to 0$:

(1) The total cross section scales with ε^{-1} and thus becomes infinite (or, equivalently, the mean free path goes to zero).
(2) The absorption cross section scales with ε and thus goes to zero.
(3) The source scales with ε and thus goes to zero to properly normalize the solution.

Because both the mean distance between collisions and the probability of absorption go to zero, it is not difficult to imagine that the result will be a diffusion process for the particles.

We next assume a power series expansion in ε for the asymptotic solution:

$$\psi = \sum_{n=0}^{\infty} \psi^{(n)} \varepsilon^n \quad . \tag{27}$$

Substituting Equation (27) into Equation (26) and equating coefficients of like powers of ε, we obtain a hierarchical set of equations for the expansion coefficients in Equation (27). After slight algebraic manipulation, the leading-order equation $O(1)$ becomes

$$\psi^{(0)} = \phi^{(0)} \quad . \tag{28}$$

This equation simply states that the leading-order solution is isotropic, that is, independent of direction. After considerable manipulation and use of Equation (28), the $O(\varepsilon)$ equation becomes

$$\psi^{(1)} = -\frac{\mu}{\sigma_t} \frac{\partial \phi^{(0)}}{\partial x} + \phi^{(1)} \quad . \tag{29}$$

The $O(\varepsilon^2)$ equation (after considerable manipulation and use of previous equations) becomes

$$\mu\left(-\frac{\mu}{\sigma_t}\frac{\partial\phi^{(0)}}{\partial x}+\phi^{(1)}\right)+\sigma_t\psi^{(2)}=\sigma_t\phi^{(2)}-\sigma_a\phi^{(0)}+Q \quad . \tag{30}$$

Averaging Equation (30) over all μ (by integration), we find that the leading-order solution, $\psi^{(0)}=\phi^{(0)}$, satisfies the following diffusion equation:

$$-\frac{\partial}{\partial x}\left(\frac{1}{3\sigma_t}\frac{\partial\phi^{(0)}}{\partial x}\right)+\sigma_a\phi^{(0)}=Q \quad . \tag{31}$$

Thus, we see that this asymptotic scaling does indeed lead to a limit in which the transport solution satisfies a diffusion equation. The effective boundary conditions satisfied by the asymptotic diffusion solution must be determined by a boundary-layer analysis beyond the scope of this discussion. It suffices to note that, with no incoming particles at the boundaries, the asymptotic diffusion solution is zero at both boundaries.

The fundamental scale length associated with the diffusion equation is the diffusion length L:

$$L=\frac{1}{\sqrt{3\sigma_a\sigma_t}}=\sqrt{\frac{\lambda_t}{3\sigma_a}} \quad . \tag{32}$$

Homogeneous solutions of Equation (31) have the form $\exp(\pm x/L)$. Note that, if we apply the asymptotic scaling defined in Equation (26) to L, we find that L is independent of ε, which is appropriate because an asymptotic scale length should not depend on ε. Further note that, since L is $O(1)$ and λ_t is $O(\varepsilon)$ in the diffusion limit, the mean free path becomes infinitely small relative to a diffusion length in the asymptotic diffusion limit. This implies that the mean free path can be arbitrarily small relative to a diffusion length in problems that are highly diffusive.

The diffusion limit for a spatially discretized transport equation is completely analogous to that for the analytic transport equation. We have shown that the transport solution satisfies an analytic diffusion equation in the asymptotic diffusion limit. By analogy, one would expect a spatially discrete transport solution to satisfy a valid spatially discrete diffusion equation in the asymptotic diffusion limit. A transport spatial-discretization scheme preserves the asymptotic diffusion limit when this occurs. In a practical sense, this means that an accurate solution can be expected in highly diffusive problems if the width of each mesh cell is small compared with a diffusion length. If a discretization scheme does not preserve the diffusion limit, one generally finds that an accurate solution can be obtained for highly diffusive problems only if the width of each cell is small with respect to a mean free path. This condition is nonphysical in the sense that the mean free path is an appropriate scale length for the transport solution in highly absorbing problems, but it is not a scale length for the transport solution in diffusive problems. More significantly, as a problem becomes increasingly diffusive, the mean free path approaches zero while the diffusion length remains constant. Thus, an arbitrarily large number of spatial cells can be required to obtain an accurate solution in highly diffusive problems if a spatial-discretization scheme does not preserve the asymptotic diffusion limit.

We next consider two spatial-discretization schemes for the transport equation and discuss their properties for diffusive problems. The first is the upwind

scheme, and the second is the diamond scheme. Although it may not be obvious, all transport discretizations are completely defined by the equations for a single spatial cell. The reason is that each spatial cell can be considered to be an independent transport domain with the incoming angular flux defined by either true boundary conditions or the outgoing angular fluxes from adjacent cells. Let us consider a cell defined over the interval $[x_{i-1/2}, x_{i+1/2}]$, and let $h = x_{i+1/2} - x_{i-1/2}$ denote the cell width. Integrating Equation (24) over this interval, we get the balance equation, which is exact:

$$\mu\left(\psi_{i+\frac{1}{2}} - \psi_{i-\frac{1}{2}}\right)\Big/ h + \sigma_{t,i}\,\psi_i = (\sigma_t - \sigma_a)\,\phi_i + Q_i \quad . \tag{33}$$

For simplicity, we have assumed a uniform grid with constant cross sections in Equation (33). Three angular fluxes appear in this equation, namely, two cell-edge values and one cell-average value. As previously noted, the incoming cell-edge angular flux is known, leaving two unknowns: the cell-average and the outgoing cell-edge angular fluxes. The balance equation provides one of two equations needed to close the system. The second equation is usually called the auxiliary equation and relates the outgoing cell-edge and cell-average angular fluxes. In the case of upwind differencing, the outgoing cell-edge angular flux is equal to the cell-average angular flux:

$$\begin{aligned} \psi_i &= \psi_{i+\frac{1}{2}} \quad \text{for } \mu > 0 \,, \\ &= \psi_{i-\frac{1}{2}} \quad \text{for } \mu < 0 \,. \end{aligned} \tag{34}$$

In the case of diamond differencing, the cell-average angular flux is the arithmetic average of the incoming and outgoing cell-edge angular fluxes:

$$\psi_i = \frac{1}{2}\left(\psi_{i+\frac{1}{2}} + \psi_{i-\frac{1}{2}}\right) \quad \text{for all } \mu \quad . \tag{35}$$

An asymptotic analysis for the upwind scheme in the thick diffusion limit yields a rather bizarre result. In particular, the upwind asymptotic solution satisfies the following difference equation:

$$\frac{1}{4h}\left(\phi_i^{(0)} - \phi_{i-1}^{(0)}\right) - \frac{1}{4h}\left(\phi_i^{(0)} - \phi_{i+1}^{(0)}\right) = 0 \quad . \tag{36}$$

If we multiply Equation (36) by $4/h$, we obtain a standard three-point cell-centered discretization for the following analytic diffusion equation:

$$-\frac{\partial^2 \phi^{(0)}}{\partial x^2} = 0 \quad . \tag{37}$$

However, comparison with Equation (31) shows that this is not the right diffusion equation. It contains no cross sections and no source! Thus, the upwind scheme does not preserve the asymptotic diffusion limit.

An asymptotic analysis of the diamond scheme in the thick diffusion limit indicates that the diamond solution satisfies the following asymptotic difference equation:

$$-\frac{1}{3\sigma_t}\left(\phi^{(0)}_{i+\frac{3}{2}} - 2\phi^{(0)}_{i+\frac{1}{2}} + \phi^{(0)}_{i-\frac{1}{2}}\right)\Big/ h^2 + \frac{\sigma_a}{4}\left(\phi^{(0)}_{i+\frac{3}{2}} + 2\phi^{(0)}_{i+\frac{1}{2}} + \phi^{(0)}_{i-\frac{1}{2}}\right) = \frac{1}{2}(Q_{i+1} + Q_i) \quad . \qquad (38)$$

This is a valid discretization scheme for the diffusion equation given in Equation (31). Thus, the diamond scheme preserves the asymptotic diffusion limit.

We next consider computational examples that will hopefully make the concept of the discrete diffusion limit concrete. To illustrate the discrete asymptotic limit, we first define a fixed initial transport problem and associate it with $\varepsilon = 1$. The problem then changes as a function of ε, according to the scaling of the total cross section, the absorption cross section, and the source given in Equation (26). Specifically, the initial problem is defined as follows:

(1) The spatial domain is the interval [0, 1], measured in centimeters, and is fixed for all ε.
(2) The transport solution satisfies vacuum boundary conditions, that is, ψ is zero at both boundaries in the incoming directions.
(3) The internal source is spatially constant with $Q = 1$ particle per cubic centimeter per second [p/(cm^3-s)].
(4) The cross sections are spatially constant with $\sigma_t = 10$ expected interactions per centimeter and $\sigma_a = 0.1$ expected absorption per centimeter.
(5) The cell thickness, h, is 0.1 centimeter, for a total of 10 spatial cells.

As previously stated, we assume that this initial problem corresponds to $\varepsilon = 1$. Then, we scale σ_t by ε^{-1}, σ_a by ε, and Q by ε. For instance, when $\varepsilon = 0.1$, we find that $\sigma_t = 100$ expected interactions per centimeter, $\sigma_a = .01$ expected absorption per centimeter, and $Q = 0.1$ p/(cm^3-s). The asymptotic transport solution to this sequence of problems satisfies Equation (31) with zero Dirichlet boundary conditions; that is, the solution is zero at both boundaries. Note that the diffusion equation is invariant to the scaling of the physical parameters, so the set of physical parameters for any value of ε may be used to evaluate the asymptotic diffusion solution. Furthermore, note that h/λ_t is scaled by ε^{-1}, so the number of mean free paths per cell becomes infinite as $\varepsilon \to 0$.

We plot the upwind and diamond solutions in Figures 10 and 11, respectively, for ε =1, 0.25, and 0.1. Figure 11 shows that the upwind solutions converge to zero with decreasing ε, in accordance with the analysis. This convergence to zero occurs because particles enter the computational domain only through the internal source Q, which is not present in the discrete asymptotic equation given by Equation (14). It can be seen from Figure 3 that the diamond solutions appear to converge to the analytic asymptotic diffusion solution given by Equation (31). However, the convergence will eventually stagnate because the mesh is fixed. The diamond solutions actually converge to the solution of Equation (38) with boundary conditions corresponding to $\phi^{(0)} = 0$ at both $x = 0$ centimeter and $x = 1$ centimeter.

We next demonstrate the excessive mesh refinement required by a scheme that does not preserve the diffusion limit. In particular, we plot the upwind solutions for the problem corresponding to $\varepsilon = 0.1$ calculated with 10, 100, and 1000 spatial

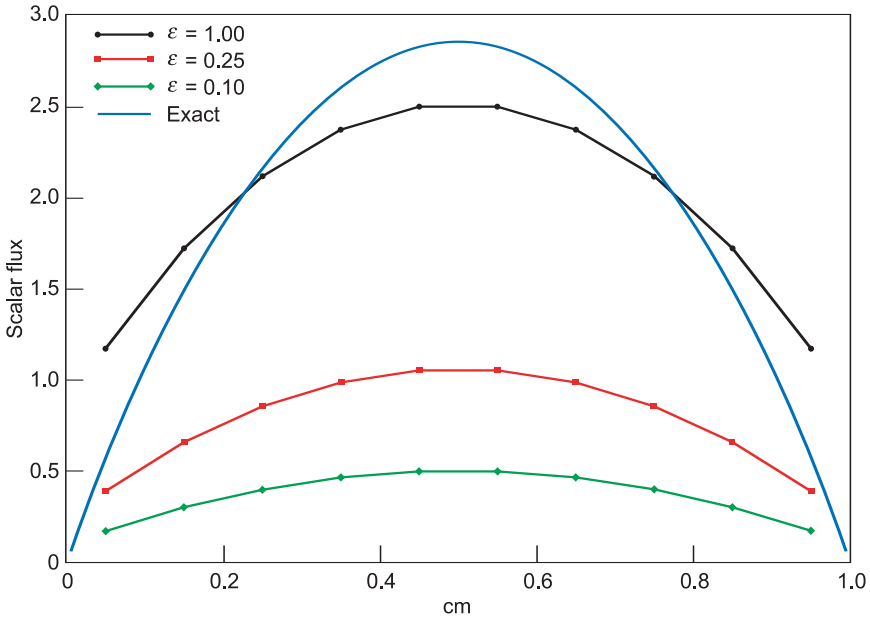

Figure 10. Solutions for the Scalar Flux in the Asymptotic Diffusion Limit with Upwind Spatial Differencing
Shown are the numerical solutions to Equation (31) for several values of ε. The "exact" analytical solution is also shown.

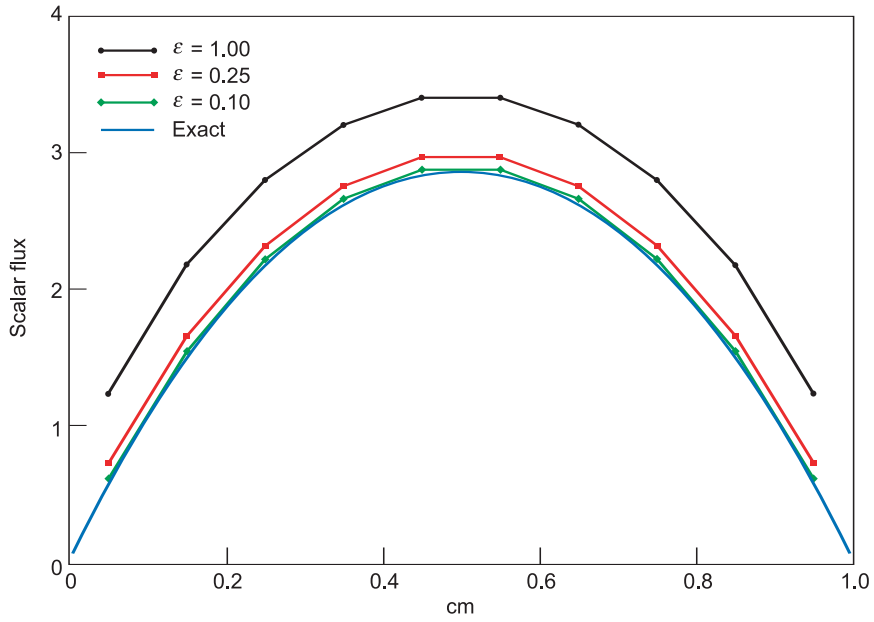

Figure 11. Solutions for the Scalar Flux in the Asymptotic Diffusion Limit with Diamond Spatial Differencing
Shown are the numerical solutions to Equation (31) for several values of ε. The "exact" analytical solution is also shown.

cells, respectively. It can be seen from Figure 12 that the upwind scheme is converging, but a small amount of error is still evident with 1000 spatial cells. The cell thickness in the 1000-cell calculation is 0.01 mean free paths. As expected, an accurate solution requires a cell width that is small when measured in mean free paths. The accuracy of the 1000-cell calculation will be maintained for smaller values of ε only if the cell width remains fixed when measured in mean free paths.

This is why schemes that do not preserve the diffusion limit can require an arbitrarily large number of mesh cells in highly diffusive problems. For instance, one would have to use 10,000 spatial cells for the $\varepsilon = 0.01$ problem to obtain essentially the same solution as with 1000 cells for $\varepsilon = 0.1$. In general, the number of cells required to maintain a given level of accuracy will be inversely proportional to ε. This is to be contrasted with the asymptotic-preserving diamond

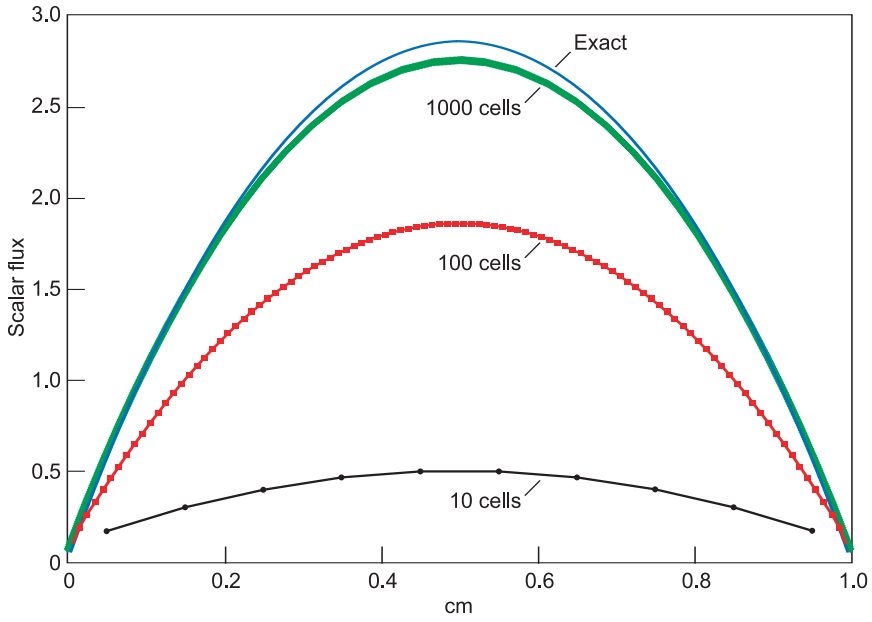

Figure 12. Solutions for the Scalar Flux in the Asymptotic Diffusion Limit with Upwind Differencing

Shown are the numerical solutions to Equation (31) for $\varepsilon = 0.1$ and different numbers of computational cells. The "exact" analytical solution is also shown.

scheme, which maintains a given level of accuracy with a fixed number of cells in the limit as $\varepsilon \to 0$, even though the cell width measured in mean free paths becomes infinite in this limit.

In summary, it is essential to use asymptotic-preserving discretization schemes in asymptotic problems whenever the scale lengths associated with the asymptotic equation are much larger than one or more scale lengths that explicitly appear in the parent equation. Schemes that are not asymptotic preserving can be prohibitively expensive to use because they require the mesh to be refined with respect to scale lengths that can be arbitrarily small compared with the scale lengths associated with the asymptotic solution. Although we have focused on the transport equation and the asymptotic diffusion limit, the basic properties that we have illustrated apply to a wide variety of physical systems. The concept of asymptotic-preserving discretizations is relatively new and not well known in the computational community. However, it can be expected to gain widespread attention in the near future because of the increasing emphasis on multiphysics/multiscale numerical simulation.

Conclusions

The common thread of the three numerical methodologies discussed in this article is the inclusion of physical insight. Perhaps, the major driving force at Los Alamos for developing such methodologies is the weapons program. However, these methods are also affecting such diverse areas as weather simulation, magnetic-confinement fusion simulations, nuclear reactor safety simulation, and aircraft design. Efforts aimed at developing and implementing such methods are ongoing within several Los Alamos programs. However, developing physically motivated numerical-discretization schemes remains a challenging task as we move toward more-accurate computer simulations of phenomena involving many types of physics. ■

Further Reading

Mimetic Discretizations for PDEs

Berndt, M., K. Lipnikov, D. Moulton, and M. Shashkov. 2001. Convergence of Mimetic Finite Difference Discretizations of the Diffusion Equation. East-West *J. Numer. Math.* **9** (4): 265.

Campbell, J. C., and M. J. Shashkov. 2001. A Tensor Artificial Viscosity Using a Mimetic Finite Difference Algorithm. *J. Comput. Phys.* **172** (2): 739.

Campbell, J. C., J. M. Hyman, and M. J. Shashkov. 2002. Mimetic Finite Difference Operators for Second-Order Tensors on Unstructured Grids. *Comput. Math. Appl*. **44** (1–2): 157.

Caramana, E. J., and M. J. Shashkov. 1998. Elimination of Artificial Grid Distortion and Hourglass-Type Motions by Means of Lagrangian Subzonal Masses and Pressures. *J. Comput. Phys*. **142** (2): 521.

Caramana, E. J., and P. P. Whalen. 1998. Numerical Preservation of Symmetry Properties of Continuum Problems. *J. Comput. Phys.* **141** (2): 174.

Caramana, E. J., M. J. Shashkov, and P. P. Whalen. 1998a. Formulations of Artificial Viscosity for Multi-dimensional Shock Wave Computations. *J. Comput. Phys.* **144** (1): 70.

Caramana, E. J., D. E. Burton, M. J. Shashkov, and P. P. Whalen. 1998b. The Construction of Compatible Hydrodynamics Algorithms Utilizing Conservation of Total Energy. *J. Comput. Phys.* **146** (1): 227.

Garimella, R. V., M. J. Shashkov, and P. M. Knupp. 2004. Triangular and Quadrilateral Surface Mesh Quality Optimization Using Local Parameterization. *Comp. Methods Appl. Mech. Eng.* **193**: 913.

Hyman, J. M., and M. Shashkov. 1997a. Adjoint Operators for the Natural Discretizations of the Divergence, Gradient and Curl on Logically Rectangular Grids. *Appl. Numer. Math.* **25** (4): 413.

———. 1997b. Natural Discretizations for the Divergence, Gradient, and Curl on Logically Rectangular Grids. *Comput. Math. Appl*. **33** (4): 81.

Hyman, J. M., and M. Shashkov. 1999a. Mimetic Discretizations for Maxwell's Equations. *J. Comput. Phys.* **151** (2): 881.

———. 1999b. The Orthogonal Decomposition Theorems for Mimetic Finite Difference Methods. *SIAM J. Numer. Anal.* **36** (3): 788.

Hyman, J. M., S. Li, P. Knupp, and M. Shashkov. 2000. An Algorithm for Aligning a Quadrilateral Grid with Internal Boundaries. *J. Comput. Phys.* **163** (1): 133.

Hyman, J., J. Morel, M. Shashkov, and S. Steinberg. 2002. Mimetic Finite Difference Methods for Diffusion Equations. *Comput. Geosci.* **6** (3): 333.

Khamayseh, A., and G. Hansen. 2000. Quasi-Orthogonal Grids with Impedance Matching. *SIAM J. Sci. Comput.* **22** (4): 1220.

Knupp, P., L. Margolin, and M. Shashkov. 2002. Reference Jacobian Optimization-Based Rezone Strategies for Arbitrary Lagrangian Eulerian Methods. *J. Comput. Phys.* **176** (1): 93.

Margolin, L. G. 1997. Introduction to An Arbitrary Lagrangian-Eulerian Computing Method for all Flow Speeds. *J. Comput. Phys.* **135**: 198.

Margolin, L. G., and J. J. Pyun. 1987. A Method for Treating Hourglass Patterns. In *Proceedings of the Fifth International Conference on Numerical Methods in Laminar and Turbulent Flow*. (Montreal, Canada, July 6–10, 1987). Edited by C. Taylor, W. G. Habashi. And M. M. Hafez. U.K.: Pineridge Press.

Margolin, L., and M. Shashkov. 1999. Using a Curvilinear Grid to Construct Symmetry-Preserving Discretizations for Lagrangian Gas Dynamics. *J. Comput. Phys.* **149** (2): 389.

Margolin, L. G., M. Shashkov, and P. K. Smolarkiewicz, 2000a. A Discrete Operator Calculus for Finite Difference Approximations. *Comp. Methods Appl. Mech. Eng.* **187** (3–4): 365.

Margolin, L., M. Shashkov, and M. Taylor. 2000b. Symmetry-Preserving Discretizations for Lagrangian Gas Dynamics. In *Proceedings of the 3rd European Conference on Numerical Mathematics and Advanced Applications*. Edited by P. Neittaanmäki, T. Tiihonen, and P. Tarvainen. p. 725. Singapore: World Scientific.

Shashkov, M. 1996. Conservative Finite-Difference Methods on General Grids. Edited by S. Steinberg. Boca Raton, FL: CRC Press.

Von Neumann, J., and R. D. Richtmyer. 1950. A Method for the Numerical Calculation of Hydrodynamic Shocks. *J. Comput. Phys.* **21** (3): 232.

Balanced Approximations for Time Integration of Multiple-Time-Scale Systems

Brackbill, J. U., and B. I. Cohen. 1985. *Multiple Time Scales*. Orlando: Academic Press.

Hirt, C. W. 1968. Heuristic Stability Theory for Finite-Difference Equations. *J. Comput. Phys.* **2** (4): 339.

Knoll, D. A., and D. E. Keyes. 2004. Jacobian-Free Newton-Krylov Methods: A Survey of Approaches and Applications. *J. Comput. Phys.* **193**: 357.

Knoll, D. A., L. Chacon, L. G. Margolin, and V. A. Mousseau. 2003. On Balanced Approximations for Time Integration of Multiple Time Scale Systems. *J. Comput. Phys.* **185**: 583.

Mousseau, V. A., D. A. Knoll, and J. M. Reisner. 2002. An Implicit Nonlinearly Consistent Method for the Two-Dimensional Shallow-Water Equations with Coriolis Force. *Mon. Weather Rev.* **130** (11): 2611.

Reisner, J., A. Wyszogrodzki, V. Mousseau, and D. A. Knoll. 2003. An Efficient Physics-Based Preconditioner for the Fully Implicit Solution of Small-Scale Thermally Driven Atmospheric Flows. *J. Comput. Phys.* **189**: 30.

Reisner, J., V. Mousseau, A. Wyszogrodzki, and D. A. Knoll. 2004. An Implicitly Balanced Hurricane Model with Physics-Based Preconditioning. (To be published in *Mon. Weather Rev*.)

Strang, G. 1968. On the Construction and Comparison of Difference Schemes. *SIAM J. Numer. Anal.* **5** (3): 506.

Warming, R. F., and B. J. Hyett. 1974. The Modified Equation Approach to the Stability and Accuracy Analysis of Finite-Difference Methods. *J. Comput. Phys*. **14** (2): 159.

Asymptotic-Preserving Discretization Schemes

Adams, M. L. 2001. Discontinuous Finite Element Transport Solutions in Thick Diffusive Problems. *Nucl. Sci. Eng.* **137**: 298.

Adams, M. L., and P. F. Nowak. 1998. Asymptotic Analysis of a Computational Method for Time- and Frequency-Dependent Radiative Transfer. *J. Comput. Phys.* **146** (1): 366.

Larsen, E. W., and J. E. Morel. 1989. Asymptotic Solutions of Numerical Transport Problems in Optically Thick, Diffusive Regimes II. *J. Comput. Phys.* **83** (1): 212.

Larsen, E. W., J. E. Morel, and W. F. Miller Jr. 1987. Asymptotic Solutions of Numerical Transport Problems in Optically Thick, Diffusive Regimes. *J. Comput. Phys.* **69** (2): 283.

Lowrie, R. B., and J. E. Morel. 2002. Methods for Hyperbolic Systems with Stiff Relaxation. *Int. J. Numer. Methods Fluids* **40**: 413.

Morel, J. E., T. A. Wareing, and K. Smith. 1996. A Linear-Discontinuous Spatial Differencing Scheme for Sn Radiative Transfer Calculations. *J. Comput. Phys.* **128** (2): 445.

For further information, contact Dana Knoll (505) 667-7467 (nol@lanl.gov) or Len Margolin (505) 665-1947 (len@lanl.gov).

Erratum to "Photoelectron Spectroscopy of Alpha- and Delta-Plutonium"
Los Alamos Science **26**: 168, 2000
A. J. Arko, J. J. Joyce, L. A. Morales, J. H. Terry, and R. K. Schulze

Some of the plutonium research presented in the article was conducted at the Advanced Light Source (ALS), Lawrence Berkeley National Laboratory. The ALS work was performed as a multi-institutional collaboration. In addition to the authors listed for the ALS work (J. H. Terry and R. K. Schulze), we would like to acknowledge their coworkers, who were Jim Tobin of Lawrence Livermore National Laboratory; Tom Zocco and Doug Farr of Los Alamos National Laboratory; David Shuh, Eli Rotenberg and Keith Heinzelman of Lawrence Berkeley National Laboratory; and Peter Boyd of Boyd Technologies. Further details of this portion of the plutonium research are available through the following publications: J. Terry, R. K. Schulze, J. D. Farr, T. Zocco, K. Heinzelman, E. Rotenberg, D. K. Shuh, G. van der Laan, D. A. Arena, and J. G. Tobin. 2002. 5f Resonant Photoemission from Plutonium. *Surf. Sci. Lett.* **499**: L141; J. G. Tobin, B. W. Chung, R. K. Schulze, J. Terry, J. D. Farr, D. K. Shuh, K. Heinzelman, E. Rotenberg, G. D. Waddill, and G. van der Laan. 2003. Resonant Photoemission in *f*-Electron Systems: Pu and Gd. *Phys. Rev. B* **68**: 155109.